The Diagonal Horn as a Sub-Millimeter Wave Antenna

Joakim F. Johansson, *Member, IEEE,* and, Nicholas D. Whyborn

Abstract—The far-field radiation pattern of a diagonal horn has been calculated by aperture integration. The radiation patterns for a 4 × 4 diagonal horn array, measured at 100 GHz, agree very well with the theoretical predictions. The aperture electric field was also expanded into Gauss–Hermite modes. The results indicate that the fraction of the power radiated into the fundamental Gaussian mode is about 84%. About 10% of the power is radiated in the cross-polarized component.

Fig. 1. A diagonal horn made in the split-block technique.

I. INTRODUCTION

COMMONLY used millimeter wave feed antennas, e.g., corrugated horns, become very difficult to realize at sub-millimeter wavelengths. Corrugated horns radiate an almost perfect Gaussian beam [1], but the tolerances needed are at the limit of what can be achieved using normal fabrication methods. Some other feed types are easier to make, but, as always, there is no such thing as a free lunch. Pyramidal and conical horns exhibit a lack of symmetry in the cardinal planes of the radiation pattern which makes them less suitable for launching Gaussian beams. The pyramidal horn has the added inconvenience of astigmatism, i.e., the phase centers for the *E*- and *H*-planes do not generally coincide (cf. [2]). The need for an alternative to these horns at sub-millimeter wavelengths is evident.

We have investigated the so-called diagonal horn (cf. [2]–[4]), and it seems to be an interesting candidate for sub-millimeter feeds. The diagonal horn antenna is shown in the following sections to be quite an efficient Gaussian beam launcher. One marked advantage with this horn type is the ease with which it can be machined. When using waveguide technology at millimeter and sub-millimeter wavelengths it is quite common that the mixer is made using a split-block technique. The block is machined in two pieces, and the waveguide is formed by milling a square cross-section channel in both halves. The losses are small for the TE_{10} mode since the split occurs along the center of the broad walls of the waveguide. The diagonal horn inherently lends itself to the split-block technique (see Fig. 1).
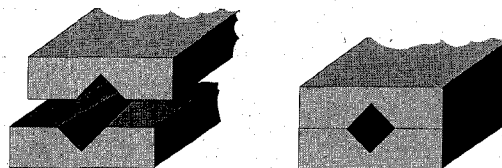
Another way to manufacture the diagonal horn would be to use the etched silicon techniques pioneered by Rebeiz *et al.* [5]. The diagonal horn could then be utilized far into the THz regime.

In addition to the above-mentioned fabrication incentives, the high packing density (while maintaining a high coupling efficiency to a Gaussian beam), and the low interaction between the horns in an array, make the diagonal horn especially attractive for focal plane imaging applications.

II. THE DIAGONAL HORN

The diagonal horn has the following electric field distribution in the aperture [2]–[4] (see Fig. 2 for reference):

$$E_{ap} = E_o \left[\hat{x} \cos \frac{\pi y}{2a} + \hat{y} \cos \frac{\pi x}{2a} \right] e^{jk\delta}$$

$$|x| < a, \quad |y| < a$$

$$k\delta = \frac{2\pi}{\lambda} \left[\frac{2a^2 - x^2 - y^2}{2L} \right]. \tag{1}$$

This means that the field consists of two orthogonal TE_{10} modes, having power equally distributed between them. This set of modes must somehow be excited. Love [3] used a circular transition from TE_{10}, but the transition seems rather uncritical, and we have found that a 'direct' transition from rectangular waveguide works well enough for most purposes (see Fig. 3).

The aperture equi-phase surface can be assumed to be a sphere centered at the horn apex, and is here approximated by a paraboloid. These assumptions are probably reasonable, at least for long horns.

The aperture field is seen to have the desired symmetry properties by introducing a coordinate system rotated by 45°, as the $\xi\eta$ system in Fig. 2, and the corresponding field components can be written as
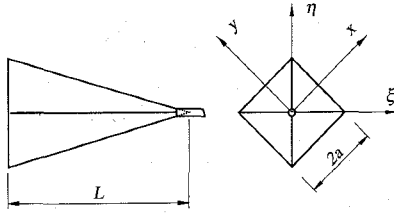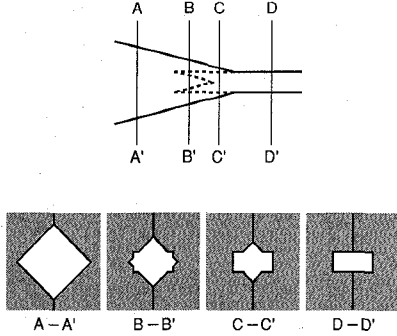
Fig. 2. The geometry of the diagonal horn.

Fig. 3. The transition from rectangular waveguide to the diagonal horn. The diagram shows cross-sections through the block at various points along the transition.

$$E_\eta = \hat{\eta} \cdot E_{ap} = \sqrt{2} E_o \cos \frac{\pi \xi}{2\sqrt{2}a} \cos \frac{\pi \eta}{2\sqrt{2}a} e^{jk\delta}$$

$$= \frac{E_o}{\sqrt{2}} \left[\cos \frac{\pi y}{2a} + \cos \frac{\pi x}{2a} \right] e^{jk\delta}$$

$$E_\xi = \hat{\xi} \cdot E_{ap} = \sqrt{2} E_o \sin \frac{\pi \xi}{2\sqrt{2}a} \sin \frac{\pi \eta}{2\sqrt{2}a} e^{jk\delta}$$

$$= \frac{E_o}{\sqrt{2}} \left[\cos \frac{\pi y}{2a} - \cos \frac{\pi x}{2a} \right] e^{jk\delta}. \tag{2}$$

The co-polarized aperture field (η-directed) is symmetric with respect to the $\xi\eta$ coordinate system. The cross-polarized aperture field component (ξ-directed) is anti-symmetric, and the feed thus has no boresight cross-polarization (note that we here use the so-called Ludwig's 1st definition [6] for the polarization, as it is more appropriate for source fields). The aperture field components are shown in Fig. 4. The fraction of the power which is radiated into the cross-polarized part can be calculated by integrating the power in the fields in (2) over the aperture, and the result is

$$\frac{P_{cr}}{P_{co} + P_{cr}} = \frac{1 - \frac{8}{\pi^2}}{2} \approx 0.0947153. \tag{3}$$

The cross-polarized part is thus quite large ($\approx$ 10%), which might be excessive for some applications. However, in many cases, this cross-polarized component could be dumped in a termination through the use of a polarizing grid. The loss incurred by absorbing the cross-polarized component is then $\approx$ 0.43 dB.
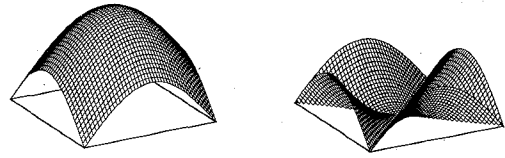

Fig. 4. The magnitude of the co- (left) and cross-polarized (right) electric field at the aperture of the horn.

III. THE RADIATION PATTERN

The radiation pattern for the diagonal horn can be found by solving the aperture integral for the equivalent electric and magnetic source distribution (cf. [4], [7]). The radiation patterns for the co- and cross-polarized components (according to Ludwig's 3rd definition [6]) are given by

$$F_{co}(\theta, \phi) = C \frac{1 + \cos \theta}{2} \left[\mathcal{P} \left[\theta, \phi + \frac{\pi}{4} \right] \right.$$
$$\left. + \mathcal{P} \left[\theta, \phi - \frac{\pi}{4} \right] \right]$$

$$F_{cr}(\theta, \phi) = C \frac{1 + \cos \theta}{2} \left[\mathcal{P} \left[\theta, \phi + \frac{\pi}{4} \right] \right.$$
$$\left. - \mathcal{P} \left[\theta, \phi - \frac{\pi}{4} \right] \right]$$

$$\mathcal{P}[\theta, \phi] = \mathcal{K}[M, u \sin \phi] \left\{ \mathcal{K} \left[M, u \cos \phi + \frac{\pi}{2} \right] \right.$$
$$\left. + \mathcal{K} \left[M, u \cos \phi - \frac{\pi}{2} \right] \right\} \tag{4}$$

where the parameters u and M and the auxiliary function $\mathcal{K}$ are given by

$$u = 2\pi \frac{a}{\lambda} \sin \theta \tag{5a}$$

$$M = \frac{\pi a^2}{\lambda L} \tag{5b}$$

$$\mathcal{K}[\alpha, \beta] = \int_{-1}^{+1} e^{+j\beta t} e^{-j\alpha t^2} dt. \tag{5c}$$

The integral in (5c) can be expressed in the well-known Fresnel integrals, or alternatively, the complex error function (cf. [8]).

A normalized graph for the E/H-plane radiation pattern versus the aperture phase error parameter M is shown in Fig. 5.

IV. MEASUREMENTS

In order to test the theoretical predictions, an array of diagonal horns was manufactured and the radiation patterns were measured. The array is shown in Fig. 6. The horns in the array had the following dimensions (see Fig. 2): $2a = 14.0$ mm and $L = 55.0$ mm.

The respective horns are fed by standard waveguide (IEC R-900) and the back side hole patterns match
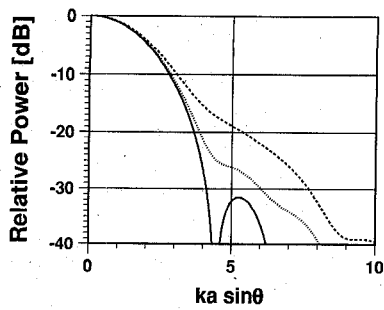
Fig. 5. Normalized radiation patterns for the E/H-planes of a diagonal horn. The curves represent $M = 0$ (solid), $\pi/4$ (dotted), and $\pi/2$ (dashed). The "obliquity factor" $(1 + \cos\theta)$ is omitted.
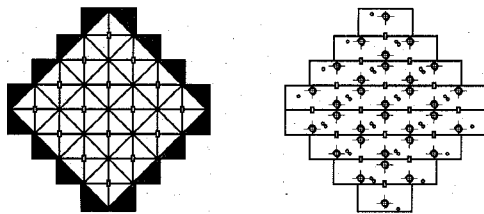

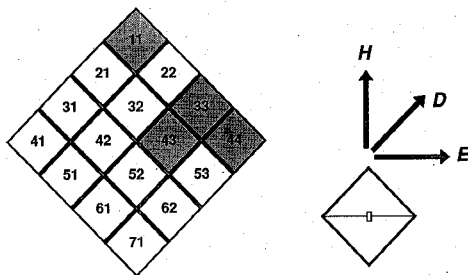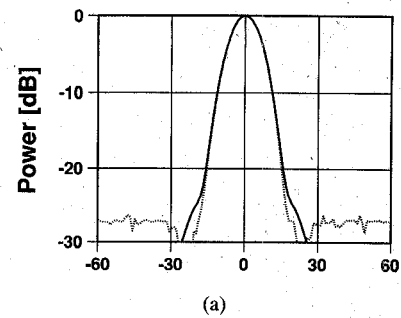Fig. 6. Front (left) and back (right) view of the diagonal horn array.

Fig. 7. The enumeration of the array elements and the plane definitions. The measured horns are shaded.

(a)

(b)

(c)

(d)

Fig. 8. (a) Comparison between the measured (dotted) and theoretical (solid) co-pol H-plane radiation patterns. (b) Comparison between the measured (dotted) and theoretical (solid) co-pol E-plane radiation patterns. (c) Comparison between the measured (dotted) and theoretical (solid) co-pol D-plane radiation patterns. (d) Comparison between the measured (dotted) and theoretical (solid) cross-pol D-plane radiation patterns.

"standard" flanges. A waveguide detector is bolted to one of the ports on the back side, with the remaining fifteen ports left open. The patterns were measured in an anechoic chamber using a computerized antenna measurement system.
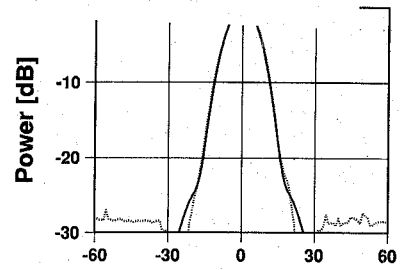
The E-, D- (45°), and H-plane co-pol patterns, as well as the D-plane cross-pol patterns were measured for four of the sixteen horns in the array (see Fig. 7 for reference) at a frequency of 99 GHz ($\lambda \approx 3.03$ mm). The patterns for element #33 are shown in Fig. 8(a)–(d). The figures show an excellent agreement between the measured and the theoretical radiation patterns. The measurement noise floor is about −30 dB.

The D-plane cross-pol component in Fig. 8(d) is a little bit asymmetrical, and shows on-axis cross-polarization. The origins of these non-idealities are probably to be found in the difficulty to accurately set up the antennas at 100 GHz and polarization impurities in the transmitting horn. Fig. 8(d) shows that the peak cross-polarized level is predicted to within half a dB.
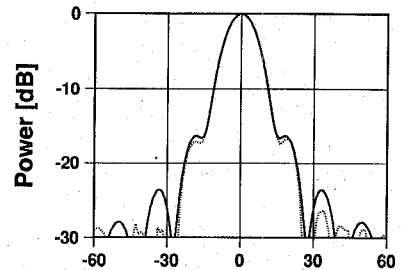
The horns do not seem to be especially influenced by being embedded in an array. Fig. 9 shows a comparison
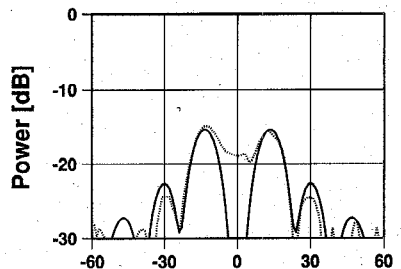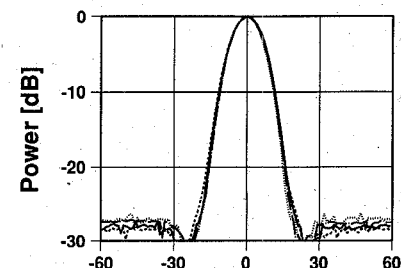

Fig. 9. Comparison between the measured co-pol H-plane radiation patterns for four different diagonal horn array elements (#11, #33, #43, and #44 in Fig. 7).

between four H-plane element patterns. The uniformity is excellent, and one can thus safely use the horns in such an array without deteriorating the radiation patterns.

V. A GAUSSIAN MODE MODEL

A powerful technique to study the radiation pattern of an aperture antenna is to expand the aperture field into Gauss–Hermite or Gauss–Laguerre functions (cf. [1], [9], [10]).

The electric field for a well-collimated beam radiating along the z axis can be written as

$$
\begin{aligned}
E(x, y, z) = \frac{w_A}{w(z)} &\exp\{-jk[z - z_A]\} \\
&\cdot \exp\{j[\Phi(z) - \Phi_A]\} \\
&\cdot \exp\{-jk[x^2 + y^2]/2R(z)\} \\
&\cdot \sum_{m=-\infty}^{\infty} \sum_{n=-\infty}^{\infty} \mathcal{K}_{mn} \\
&\cdot \exp\{j(m+n)[\Phi(z) - \Phi_A]\} \\
&\cdot \tilde{H}_m\left[\frac{\sqrt{2}x}{w(z)}\right] \tilde{H}_n\left[\frac{\sqrt{2}y}{w(z)}\right]
\end{aligned}
\tag{6}
$$

where a modified Hermite function, defined by

$$
\tilde{H}_m(x) \triangleq \frac{e^{-(x^2/2)}}{\sqrt{2^m m!}} H_m(x)
\tag{7}
$$

is used to obtain a compact notation. The beam parameters in (6) are given by (cf. [10]):

$$
w(z) = w_o \sqrt{1 + [z/z_c]^2}
$$

$$
R(z) = z[1 + [z_c/z]^2], \quad z_c = \frac{\pi w_o^2}{\lambda}
$$

$$
\Phi(z) = \arctan \frac{z}{z_c}
\tag{8}
$$

where w denotes the beam waist radius, R the phase radius of curvature, z_c the confocal distance, and Φ the so-called phase slip. Note that whereas w and R are common to all modes, the phase slip Φ is progressively multiplied for higher order modes (cf. (6)).

If one now has an aperture field E_A where most of the phase variation can be contained in a spherical phase factor, viz.:

$$
\begin{aligned}
E_A(x, y) &= E(x, y, z_A) \\
&= g(x, y) \exp\{-jk[x^2 + y^2]/2R_A\}
\end{aligned}
\tag{9}
$$

then (6) collapses into a very convenient form. Using the orthogonality properties of Hermite polynomials [8], and some algebraic manipulation, the coefficients $\mathcal{K}_{mn}$ are found to be

$$
\mathcal{K}_{mn} = \frac{2}{\pi w_A^2} \int\int_{-\infty}^{\infty} g(x, y) \, \tilde{H}_m\left[\frac{\sqrt{2}x}{w_A}\right]
$$

$$
\cdot \tilde{H}_n\left[\frac{\sqrt{2}y}{w_A}\right] dx \, dy.
\tag{10}
$$

If now the $g(x, y)$ function is real-valued, one avoids all the numerical problems due to rapid phase variations in the integrand. The diagonal horn has no phase variation over the aperture except for the spherical part. It thus lends itself to this Gauss–Hermite analysis. The $g(x, y)$ functions for the co- and cross-pol parts are given by E_η and E_ξ in (2).

The mode fractional power content is given by

$$
\frac{P_{mn}}{P_{\text{tot}}} = \frac{\pi w_A^2}{2} \frac{|\mathcal{K}_{mn}|^2}{\int\int_{-\infty}^{\infty} |g(x, y)|^2 \, dx \, dy}
\tag{11}
$$

and the results for the diagonal horn are the following expressions:

$$
\begin{aligned}
\frac{P_{mn}^{co}}{P_{\text{tot}}} = \frac{64}{\pi} \frac{a^2}{w_A^2} &\left| \int_0^1 \int_0^{1-u} \cos\frac{\pi u}{2} \cos\frac{\pi v}{2} \right. \\
&\left. \cdot \tilde{H}_m\left[\frac{2a}{w_A}u\right] \tilde{H}_n\left[\frac{2a}{w_A}v\right] du \, dv \right|^2
\end{aligned}
$$

$$
\text{even } m, n
\tag{12a}
$$

$$
\begin{aligned}
\frac{P_{mn}^{cr}}{P_{\text{tot}}} = \frac{64}{\pi} \frac{a^2}{w_A^2} &\left| \int_0^1 \int_0^{1-u} \sin\frac{\pi u}{2} \sin\frac{\pi v}{2} \right. \\
&\left. \cdot \tilde{H}_m\left[\frac{2a}{w_A}u\right] \tilde{H}_n\left[\frac{2a}{w_A}v\right] du \, dv \right|^2
\end{aligned}
$$

$$
\text{odd } m, n.
\tag{12b}
$$

The choice of the ratio w_A/a is in principle arbitrary, but a logical choice is to maximize the fundamental mode coupling, i.e.:

$$
\frac{\partial \eta_{\text{Gauss}}}{\partial \frac{w_A}{a}} = 0, \quad \eta_{\text{Gauss}} = \frac{P_{00}^{co}}{P_{\text{tot}}}.
\tag{13}
$$

The maximum coupling, $\eta_{\text{Gauss}} \approx 0.843025$, is achieved for $w_A/a \approx 0.863191$. The diagonal horn thus has quite a high fundamental Gaussian mode content. The mode content for a few higher order co-polar and cross-polar components is shown in Table I.

The fundamental Gaussian mode coupling for the conical horn is $\eta_{\text{Gauss}} \approx 0.8662$ for $w_A/a \approx 0.768$ [11], where a denotes the aperture radius. The diagonal horn achieves almost the same coupling, but to a larger waist

TABLE I
THE FRACTIONAL MODE POWER CONTENT IN THE *mn*th MODE

Order [mn]	Co-Pol Mode Power	Order [mn]	Cross-Pol Mode Power
00	0.8430	11	0.04848
02 (= 20)	$3.655 \cdot 10^{-18}$	13 (= 31)	0.007725
04 (= 40)	0.005405	15 (= 51)	0.0004141
22	0.01620	33	$6.037 \cdot 10^{-5}$
24 (= 42)	0.003339	35 (= 53)	0.001545
44	$1.562 \cdot 10^{-5}$	55	0.002060

The power fraction for the remaining higher order modes is 2.86% and 2.47% for the co- and the cross-polarized components, respectively.
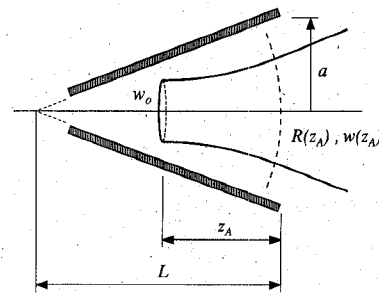

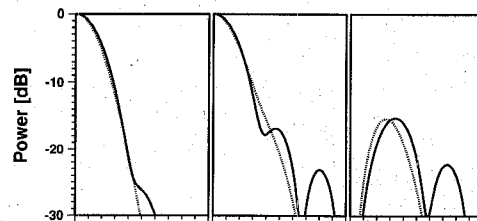Fig. 10. The geometry of the equivalent Gaussian beam.

Fig. 11. A comparison between the radiation patterns for the aperture integration method (solid) and the Gaussian beam model (dotted) for $M = \pi/4$ ($\Phi \approx 30°$). The panels show the normalized co-pol E/H-plane (left), co-pol D-plane (center), and cross-pol D-plane (right) patterns.

radius, and hence can achieve a higher packing density than the conical horn. The corrugated horn has a coupling of $\eta_{\text{Gauss}} \approx 0.9792$ for $w_A/a \approx 0.6435$ [1], and it is evident that high coupling efficiency is achieved at the cost of increased aperture size (cf. [13], [14]).

Once the optimum waist radius is known, it is easy to find the equivalent Gaussian beam parameters. If one assumes the following (see Fig. 10 for reference):

$$w_A = w_o \sqrt{1 + [z_A/z_c]^2} = \kappa a, \quad z_c = \frac{\pi w_o^2}{\lambda}$$

$$R_A = z_A[1 + [z_c/z_A]^2] = L$$

$$\Phi_A = \arctan \frac{z_A}{z_c} = \arctan \kappa^2 M, \quad M = \frac{\pi a^2}{\lambda L} \quad (14)$$

then some algebraic manipulations will yield the results

$$w_o = \frac{\kappa a}{\sqrt{1 + \tan^2 \Phi_A}} \quad z_A = \frac{L}{1 + \cos^2 \Phi_A}. \quad (15)$$

Table I showed that there are just a few terms that contain a significant part of the power, namely the 00, 11, and 22 terms (contain a total of 90.8% of the power). It is hence possible to devise a simple model for the radiation pattern of the diagonal horn, using these three modes. The far-field radiation pattern is then given by (except for an unimportant constant):

$$F_{co}(\theta, \varphi) \approx e^{-2\rho^2}|\mathcal{K}_{00} + \tfrac{1}{2}\mathcal{K}_{22} e^{-j4\Phi_A}$$

$$\cdot [4\rho^2 \cos^2 \varphi - 1][4\rho^2 \sin^2 \varphi - 1]|^2$$

$$F_{cr}(\theta, \varphi) \approx e^{-2\rho^2}|\mathcal{K}_{11} 4\rho^2 \sin \varphi \cos \varphi|^2$$

$$\rho = \frac{\pi w_o}{\lambda} \tan \theta \quad (16)$$

where the mode coefficients are given by

$$\frac{\mathcal{K}_{11}}{\mathcal{K}_{00}} \approx 0.239816, \quad \frac{\mathcal{K}_{22}}{\mathcal{K}_{00}} \approx -0.138628. \quad (17)$$

Fig. 11 shows a comparison between the simplified Gaussian model and the "exact" model from Section III.

The agreement is good in the main lobe for levels down to about -25 dB in the E- and H-planes and fair above about -15 dB in the D-plane. The simplified Gaussian model fails to predict the shoulders in the D-plane, but can still be used for preliminary quasi-optical design work. For a more detailed analysis one would have to use many modes to correctly predict the aperture efficiency when feeding, for example, a Cassegrainian (cf. [12]).

VI. CONCLUSION

The diagonal horn antenna has been theoretically investigated. The model using aperture integration yields an excellent agreement with measured data. The horn has a high fundamental Gaussian mode content ($\approx 84\%$). The design lends itself to conventional millimeter and submillimeter construction methods, such as the split-block technique.

The very weak interactions that were seen in the array measurements indicate that the diagonal horn antenna is a strong candidate for focal plane imaging arrays.
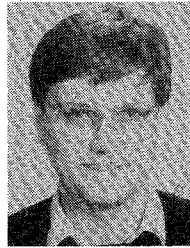
REFERENCES

[1] R. Wylde, "Optics and corrugated feedhorns," *Proc. Inst. Elec. Eng.*, vol. 131, pt. H, no. 4, pp. 258–262, Aug. 1984.

[2] E. I. Muehldorf, "The phase center of horn antennas," *IEEE Trans. Antennas Propagat.*, vol. AP-18, no. 6, pp. 753–760, Nov. 1970.

[3] A. W. Love, "The diagonal horn antenna," *Microwave J.*, vol. V, pp. 117–122, Mar. 1962.

[4] E. A. Wolff, *Antenna Analysis*. New York: Wiley, 1966.

[5] G. M. Rebeiz, D. P. Kasilingam, Y. Guo, P. A. Stimson, and D. B. Rutledge, "Monolithic millimeter-wave two-dimensional horn imaging arrays," *IEEE Trans. Antennas Propagat.*, vol. 38, no. 9, pp. 1473–1482, Sept. 1990.

[6] A. C. Ludwig, "The definition of cross polarization," *IEEE Trans. Antennas Propagat.*, vol. AP-21, no. 1, pp. 116–119, Jan. 1973.

[7] C. A. Balanis, *Antenna Theory Analysis and Design*. New York: Harper & Row, 1982.

[8] M. Abramowitz and I. A. Stegun, *Handbook of Mathematical Functions*, 9th printing, New York: Dover.

[9] J. A. Murphy and R. Padman, "Phase centers of horn antennas using Gaussian beam mode analysis," *IEEE Trans. Antennas Propagat.*, vol. 38, no. 8, pp. 1306–1310, Aug. 1990.

[10] P. F. Goldsmith, "Quasi-optical techniques at millimeter and submillimeter wavelengths," ch. 5 in *Infrared and Millimeter Waves*, vol. 6, K. Button, Ed., New York: Academic, 1982, pp. 277–343.

[11] J. A. Murphy, "Aperture efficiencies of large axisymmetric reflector antennas fed by conical horns," *IEEE Trans. Antennas Propagat.*, vol. 36, no. 4, pp. 570–575, Apr. 1988.

[12] R. Padman, J. A. Murphy, and R. E. Hills, "Gaussian mode analysis of Cassegrain antenna efficiency," *IEEE Trans. Antennas Propagat.*, vol. AP-35, no. 10, pp. 1093–1103, Oct. 1987.

[13] K. S. Yngvesson, J. F. Johansson, Y. Rahmat-Samii, and Y. S. Kim, "Realizable feed-element patterns and optimum aperture efficiency in multi-beam antenna systems," *IEEE Trans. Antennas Propagat.*, vol. 36, no. 11, pp. 1637–1641, Nov. 1988.

[14] J. F. Johansson, "Theoretical limits for aperture efficiency in multi-beam antenna systems," Research Rep. No. 161, Department of Radio and Space Science, Chalmers University of Technology, Gothenburg, Sweden, 1988.
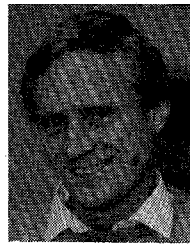
Joakim F. Johansson (S'83–M'88) was born in Töllsjö, Sweden, on November 3, 1959. He received the degrees of Civilingenjör ($\approx$ M.Sc.), Tekn. Lic., and Tekn. Dr. (Ph.D.) in electrical engineering from Chalmers University of Technology, Gothenburg, Sweden, in 1983, 1986, and 1988, respectively.

He is currently a Research Fellow at the Department of Radio & Space Science with Onsala Space Observatory, Chalmers University, doing research on millimeter and sub-millimeter wave radio astronomy instrumentation and quasi-optics. He has worked on theory and experiments in the field of focal plane imaging using tapered slot antennas, as well as EM moment method computer programs.

Dr. Johansson is Treasurer of the MTT/AP Chapter of the IEEE Swedish Section. He is a member of Eta.

Nicholas D. Whyborn was born in Redhill, Surrey, England, on October 16, 1958. He received the degrees of B.Sc.(Hons.) in Physics and D.A.S.Sc. in Radio Astronomy from Manchester University in 1981 and 1982, respectively.

He is currently with the Department of Radio & Space Science with Onsala Space Observatory, Chalmers University, doing research in the fields of millimeter and sub-millimeter wave radio astronomy and instrumentation. He has developed several receiver systems for the SEST (Sweden ESO Sub-millimeter Telescope) radio astronomy observatory at 115, 230, and 350 GHz.